LARGE EDDY SIMULATIONS OF A HYDROGEN-AIR EXPLOSION IN AN OBSTRUCTED CHAMBER USING ADAPTIVE MESH REFINEMENT

Vanbersel, B.[1], Meziat Ramirez, F.A.[1,2], Vermorel, O.[1], Jaravel, T.[1], Douasbin, Q.[1] and Dounia, O.[1]
[1] CERFACS, CFD Team, Toulouse, Cedex 01 31057, France, vanbersel@cerfacs.fr
[2] Air Liquide – Paris Innovation Campus, Les Loges-en-Josas, 78354, France

ABSTRACT

Following the growing use of hydrogen in the industry, gas explosions have become a critical safety issue. Computational Fluid Dynamic (CFD) and in particular the Large Eddy Simulation (LES) approach have already shown their great potential to reproduce such scenarios with high fidelity. However, the computational cost of this approach is an obvious limiting factor, since fine grid resolutions are often required in the whole computational domain to ensure a correct numerical resolution of the deflagration front all along its propagation. In this context, Adaptive Mesh Refinement (AMR) is of great interest to reduce the computational cost, as it allows to dynamically refine the mesh throughout the explosion scenario, only in regions where Quantities of Interest (QoI) are detected. This study aims to demonstrate the strong potential of AMR for the LES of explosions. The target scenario is a hydrogen-air explosion in the GraVent explosion channel [1]. Using the massively parallel Navier-Stokes compressible solver AVBP, a reference simulation is first obtained on a uniform and static unstructured mesh. The comparison with the experiments shows a good agreement in terms of absolute flame front speed, overpressure and flow visualisation. Then, an AMR simulation is performed targeting the same resolution as the reference simulation only in regions where QoI are detected, i.e., inside the reaction zones and vortical structures. Results show that the accuracy of the reference simulation is recovered with AMR for only 12% of its computational cost.

1.0 INTRODUCTION

Storage of highly energetic fuels, such as hydrogen, entails safety issues, including explosion hazards, particularly in confined environments. To analyse risk scenarios, understand the underlying physical mechanisms and eventually prevent accidents, high-fidelity numerical simulations can be a valuable tool. The main issue with the CFD simulations of deflagrations is the high disparity between the scales of the geometries involved, of the order of meters, and the physical scales of the flame thickness and turbulent structures, of the order of micrometers. With the increase of computational power, Large Eddy Simulations (LES) are now a credible alternative to URANS for the study of deflagrations [2]. However, accurate LES require to resolve structures down to a reasonably fine scale. Additionally, in a deflagration scenario, the flame front is very localized in space but can propagate through almost the entire computational domain. In static mesh context, this implies the use of a uniformly fine grid throughout the domain. This results in a prohibitive computational burden for large-scale configurations. In this context, the use of Adaptive Mesh Refinement (AMR) can be of great interest to reduce the computational cost, by dynamically refining the mesh all along the flame propagation only in regions where Quantities of Interest (QoI) are detected, referred to as Regions of Interest (RoI). The present study focuses on LES of a hydrogen-air deflagration in the GraVent explosion channel [1]. Firstly, the numerical setup and a description of the AMR methodology are presented. Secondly, the experimental setup of the GraVent explosion channel is introduced. Thirdly, the results of the LES on a uniform static mesh are compared with the experiments. Finally, the AMR strategy is assessed by performing an AMR simulation, with the same resolution in the RoI, allowing for comparison with the static mesh reference case.

2.0 NUMERICAL SETUP AND AMR METHODOLOGY

The LES are performed with the massively parallel, compressible, Navier-Stokes reactive code AVBP [3] on fully unstructured tetrahedral meshes. The Lax-Wendroff convection scheme [4], second order accurate in time and space, is employed. The WALE model [5] prescribes the subgrid turbulent stresses. The Dynamic Thickening Flame model for LES is used to dynamically thicken the flame along its propagation [6], therefore ensuring a sufficient discretisation of the strong gradients present at the flame front. The efficiency function of Colin [7] is employed to model the subgrid turbulence-chemistry interactions of the thickened flame front.

Concerning mesh adaptation, various methods have been developed in the literature and cover a large range of applications. Simulations of steady-state phenomena rely on static mesh refinement, whose goal is to converge towards a mesh that verifies certain error criteria based on time-averaged physical quantities or discretization errors. However, deflagrations are transient phenomena and, thus, require adaptive mesh refinement, with on-the-fly definition of metrics and criteria for triggering the mesh adaptation. The construction of the metric can be based on different approaches. Some methods are based on physical or numerical error criteria [8]: it is a common approach for AMR which is mathematically well-posed and is fairly adapted in a DNS approach. However, in the context of LES, the definition of errors needs to account for the LES filter size, which is directly linked to the local grid size, to avoid an unaffordable degeneration of the adapted mesh towards a DNS mesh. Moreover, these errors are difficult to construct in a highly unsteady context, as they often require averaging (in space or time). Here, a feature-based AMR is considered instead, for which the mesh refinement is applied to resolve accurately critical features identified *a priori*, which define the Regions of Interest (RoI). It is well suited in the context of deflagrations, for which the main drivers of the flame acceleration process are well-known. The RoI are constructed on-the-fly through sensors based on Quantities of Interest (QoI) computed at each time step. In deflagration cases, the most salient features of the physics are the flame and turbulence that control flame acceleration (FA) phenomena and consequently the severity of the explosion. In most cases, the flame accelerates through surface variation, first due to the burnt gases expansion, then by the interaction with the vortical and turbulent structures induced by the flow and the obstacles in the fresh gases. These structures wrinkle the flame and increase its burning rate, creating a positive feedback loop between the unsteady flame and the flow hydrodynamics.

Several QoI have been used in the literature for AMR in the context of propagating flames, but most of them use dimensional quantities such as velocity, species or pressure gradients [10], vorticity [11] or heat release rate [8]. In this work, the QoI used are the following:

- The flame sensor, θ_F from the DTFLES model, using the formulation of Legier et al. [12]. Originally designed to determine where the artificial thickening should be applied, it is computed at each iteration and used to locate the flame front, where sharp species gradients and the flame reaction zone are found;

- The vortex sensor Ω, that detects the regions of the flow where the rotation rate overtakes the deformation rate, using the formulation of Liu et al. [13]. It allows for the identification of the vortical structures without depending on an arbitrary threshold, as would be the case if one were using a simpler detection criteria, such as a vorticity threshold.

These two sensors are dimensionless and bounded between zero and one. The goal of using these QoI is to have a versatile AMR setup that could be used on several configurations without any parameter tuning.

A binary mask field is used to define the metric that is fed to the AMR algorithm. In regions where any QoI is detected, whether it corresponds to the presence of the flame or the vortices, the binary mask takes the value of unity. There, a fine grid resolution Δ_x^{min} is targeted. The binary mask field vanishes in regions where no QoI are detected (Δ_x^{max} resolution for the metric). These two extreme values (Δ_x^{min}

and Δ_x^{max}) are fixed by the user and should be adapted to the geometry, relevant physics and the computational budget.

Additionally, as the flame is a propagative phenomenon, it may leave the region with fine grid resolution between two adaptation steps. This situation must be avoided as it would lead to higher discretization and interpolation errors. To ensure that the QoI do not leave the fine regions of the mesh, the mask field is dilated in space by one cell. Since the flame only propagates towards the fresh gases, the dilatation is only done in this direction. This procedure is illustrated in Fig. 1: the dilatation of the mask field results in a larger fine mesh zone ahead of the flame, in its propagation direction, i.e. the fresh gases. This allows for the flame to propagate for a longer time without the need of triggering a new mesh adaptation.
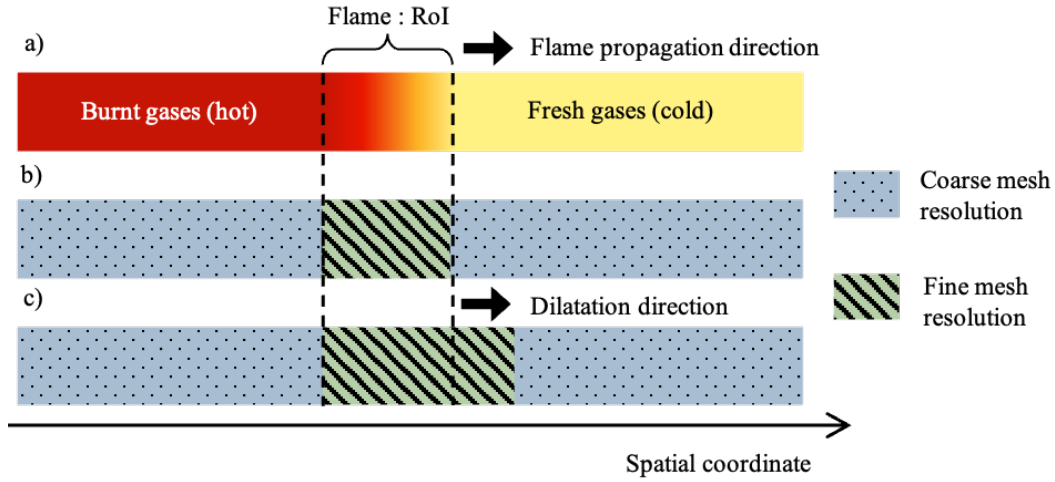
Figure 1: Schematic of the dilatation of the binary mask towards the fresh gases: (a) temperature field and flame front; (b) resulting mesh without dilatation and (c) resulting mesh with dilatation.

The constructed target metric field is given to the AMR library of YALES2 [14], which implements AMR for massively parallel unstructured computations based on the MMG3D remeshing library [15, 16]. The mesh adaptation is performed on-the-fly and coupled with the flow solver AVBP. An illustration of the QoI and the corresponding adapted mesh is shown in Fig. 2. The flame is detected on the left side of the figure, while the vortices are detected in the wake of the obstacles. The adapted mesh will be fine in the RoI and relax to a coarse mesh resolution elsewhere. The transition between fine and coarse regions of the mesh is controlled by a selected growth rate.
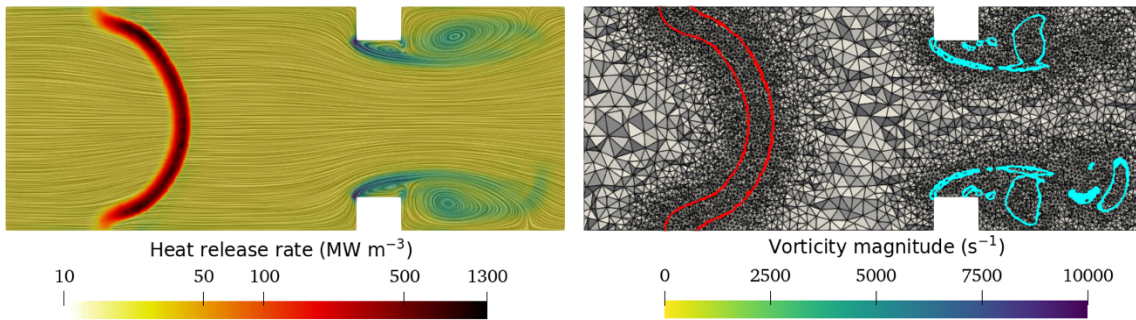

Figure 2: Illustration of the flow in a section of the GraVent explosion channel (Sections 3 and 4) together with the corresponding QoI and adapted mesh. Velocity vectors line integral convolution, coloured by vorticity magnitude, plus heat release rate (left). QoI (flame and vortices) delimited by contours (red and blue) and adapted mesh (right).

To maintain the QoI in a fine mesh region along their evolution in time and space, several mesh adaptations are needed during the simulation. A triggering criterion for the adaptation is thus needed.

Several criteria exist in the literature, from the most basic one which triggers a mesh adaptation at a user-fixed frequency [17], to more advanced criteria, based for instance on the mask field variation [9]. Most of these methods require a user-fixed threshold, that is case dependent and not known *a priori*. An automatic method, based on the objective that the RoI have to be resolved at the finest grid scale Δ_x^{min} at every time-step, is used here, as shown in Fig. 3. The flame is initially free to propagate in a fine mesh zone until, after a certain time, it reaches the end of said zone. This critical instant is detected by comparing the flame sensor field θ_F with the binary mask, which indicates where fine mesh zone is. A mesh adaptation is, then, automatically triggered and a new mesh with a fine zone encompassing the front is generated.
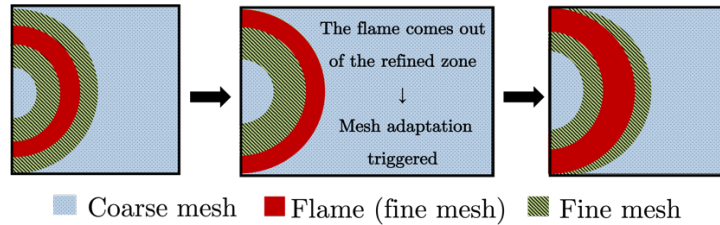
Figure 3: Principle of the automatic mesh adaptation triggering method. The flame propagates from left to right and an adaptation is triggered after the front reaches the end of the fine mesh zone.

The combination of dimensionless QoI and automatic mesh adaptation triggering method avoids a dependence on case-specific physical scales, leading to a robust AMR method that can be used on several deflagration scenarios without any user parameter modification.

3.0 GRAVENT BR30HS300 EXPERIMENTAL CONFIGURATION

The configuration studied here is the GraVent explosion chamber from TU Munich [1]. This experiment aims to represent a hydrogen leakage scenario in a confined environment with a delayed ignition. It is a closed, high aspect-ratio channel with identical, evenly spaced obstacles. The channel is initially filled with a homogeneous hydrogen-air mixture at ambient temperature and pressure. The mixture is ignited with a spark plug at the left end of the channel. Depending on the chosen operating condition, several scenarios of flame acceleration can be observed. For the most reactive mixtures, a transition to detonation may occur. A large database is available online, comprising conventional measurement techniques (time-of-arrival photodiodes and pressure transducers) as well as optical visualisation techniques (shadowgraphy and high speed OH-PLIF). Several geometrical configurations are available. The BR30hS300 chamber is studied here and presented in Fig. 4. Its dimensions are L x l x H = 5400 x 300 x 60 mm, which corresponds to a total volume of 97.2 L. It comprises a total of seven obstacles, with a blockage ratio of 30%. The complete experimental setup from TU Munich is illustrated in Fig. 5.
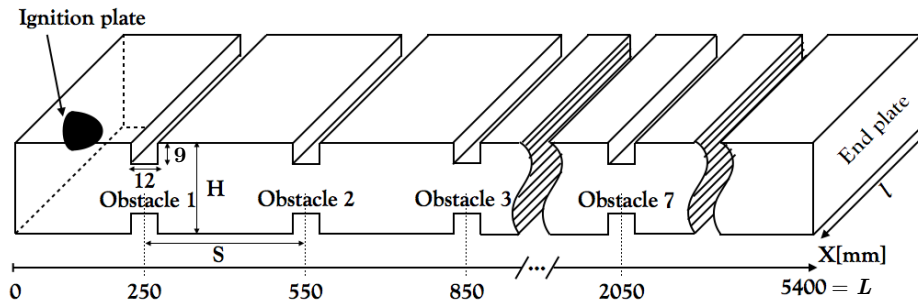

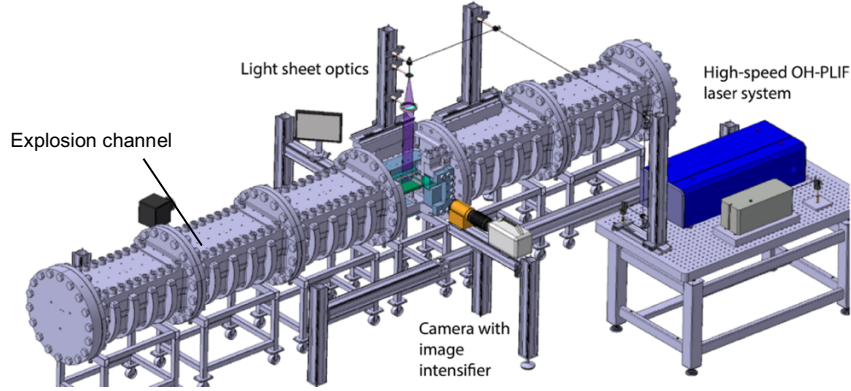Figure 4: Schematic of the GraVent BR30hS300 channel. Adapted from Dounia [18].

Figure 5: Complete GraVent experimental setup. Adapted from Boeck et al. [1].

4.0 RESULTS AND ANALYSIS

4.1 Static mesh reference simulation

The operating point studied considers a premixed hydrogen-air mixture at 17.5% H_2 by volume. For these conditions, only a fast deflagration is observed without Deflagration-to-Detonation-Transition (DDT) (Fig. 6), according to the experimental results of Boeck [19].
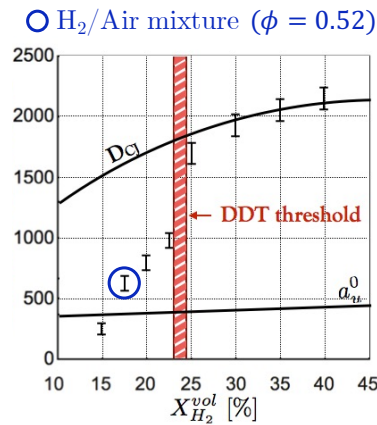

Figure 6: Experimental absolute flame front speed at the last obstacle as a function of the volume fraction of hydrogen. D_{CJ} is the detonation speed corresponding to these conditions and a_u^0 is the sound speed of the reactants at the initial conditions. Adapted from Boeck [19].

The FA mechanisms occur in the obstructed section of the channel. Therefore, as depicted in Fig. 7, the mesh is refined from the ignition point to the last obstacle (constant resolution of 1 mm) and then coarsened up to the right end (constant resolution of 2 mm). The resulting mesh is made of 379M tetrahedral elements. The Boundary Conditions (BC) are isothermal walls with law-of-the-wall treatment.
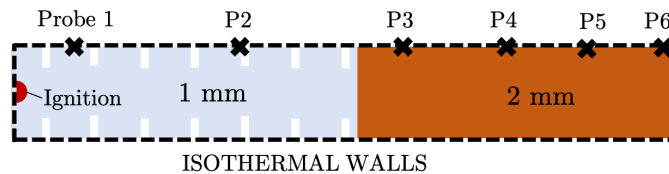

Figure 7: Edge size distribution for the static mesh and associated BC. Pressure transducers locations at the center of the top wall are indicated by crosses.

Regarding chemical kinetics, a simple, inexpensive single-step chemical scheme is built. The chemistry is fitted so that the laminar flame speed s_L^0 of a complex chemical scheme of reference [20], at the initial conditions of the deflagration $T_0 = 300$ K and $p_0 = 1$ atm, is recovered (Table 1).

Table 1: Laminar H_2-air flame characteristics at $T_0 = 300$ K and $p_0 = 1$ atm for the single-step chemical scheme.

ϕ	s_L^0 (ms^{-1})	T_{ad} (K)	δ_L^0 (m)
0.52	0.59	1657	$2.03 \cdot 10^{-4}$

The simulation is initialised through a hemispherical, 10 mm radius, kernel of burnt gases. The transition from fresh to burnt gases is done through the profiles of a 1-D planar, laminar flame, computed with the chemical kinetics solver Cantera [21].

Regarding the LES results, the validation focuses on the absolute flame front tip speed in the laboratory reference frame, together with the pressure signals at different locations along the channel (probes P1 to P6 in Fig. 7). Firstly, the flame propagation absolute speed shown in Fig. 8 reveals a very good agreement with the experimental measurements. As expected, even with such high absolute velocity levels, no DDT occurs. The LES flame speed oscillations do not appear in the experimental measurements due to the limitations in the dynamic range of the time-of-arrival photodiodes.
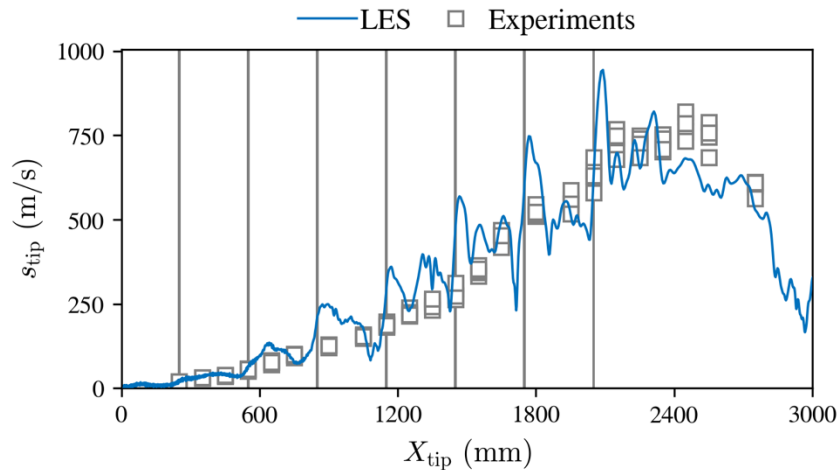

Figure 8: Flame tip absolute propagation speed s_{tip} with respect to the flame tip position along the channel X_{tip}. The position of the obstacles is indicated by vertical lines.

The pressure evolution inside the channel is directly driven by the FA. As the flame accelerates, compression waves are generated and are identified both experimentally and numerically from the pressure probe signals. These are shown in Fig. 9, highlighting that the LES manages to correctly reproduce the experimental signals. The increasingly stronger acceleration rate across each obstacle creates progressively faster compression waves, that coalesce into a strong normal shock at the exit of the last obstacle. This shock propagates in the fresh gases ahead of the flame and is reflected at the end of the chamber. The evolution of the flame and the flow due to the strong acceleration across the obstructed section of the channel can be visualized in Fig. 10. Before entering the obstructed section (Fig. 10a) and after a first laminar propagation phase, the flame shows an elongated shape, homogeneous heat release rate and no strong compression waves are observed. The influence of the flow contraction at the first obstacle can be seen at the deformed flame tip shape. Once the flame exits the obstacles (Fig. 10b), after the acceleration process, the flame front is much more wrinkled and distorted, showing higher values of heat release rate. This shows the strong impact of the turbulence produced in the wake of the obstacles on the flame. The compression waves and the formation of a strong normal shock ahead of the flame can also be visualized through the numerical schlieren.
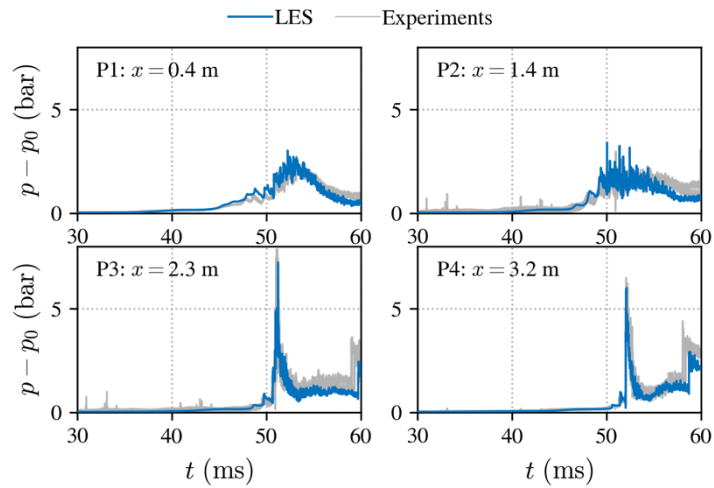
6

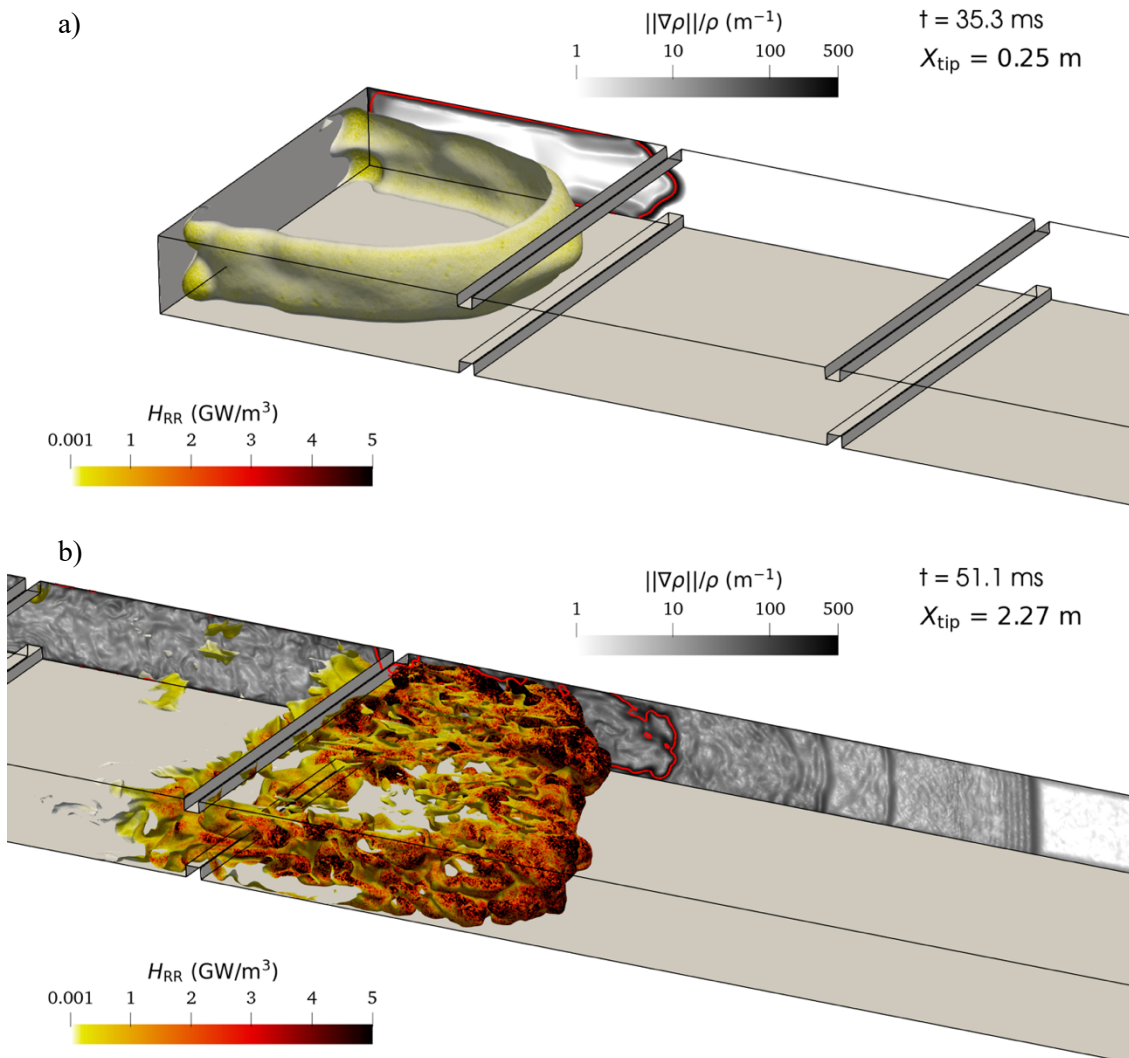Figure 9: Overpressure generated at several probe locations along the channel.

Figure 10: Visualisation of the flame before the entry (a) and at the exit (b) of the obstructed section. Flame surface coloured by heat release rate. Numerical schlieren and flame contour on mid-plane section of the channel.

4.2 AMR simulation

The LES performed on a static mesh has been validated against the experiments (the corresponding results are indicated in this section as REF). Now, an AMR simulation is performed to evaluate the capabilities of the method. The same resolution as the static uniform mesh is targeted in regions where QoI are detected ($\Delta_x^{min} = \Delta_x^{ref} = 1$ mm between the obstacles, $\Delta_x^{min} = 2$ mm after, see Fig. 7), and coarsened by a factor 5 elsewhere. This allows a fair comparison between both simulations: the goal is to recover the same level of precision as the reference simulation done on a static mesh (REF), but for a much lower computational cost. In Fig. 11, the static mesh of the REF case is compared with the first adapted AMR mesh. A huge reduction in the mesh size is observed (number of cells divided by 95).
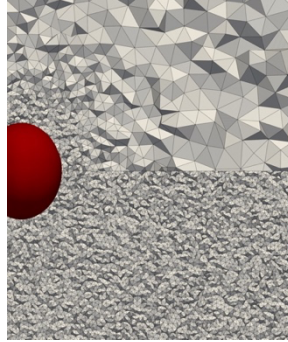

Figure 11: Initial flame kernel. Top: first mesh adapted to the initial solution (4M cells); bottom: static and uniform mesh (379M cells).

A visualisation of the adapted mesh when the flame gets close to the first obstacle is shown in Fig. 12. At this moment, the mesh has a total of 20 million elements (19 times less than in the REF case). The adapted mesh is finer in the flame front (red contours) but also around the successive obstacles, where vortices are detected in their wake (blue contours). The fine regions of the mesh encompass the RoI and adapt to their dynamic evolution on-the-fly. As shown in Fig. 13 the shape of the flame sensor is very similar between the two simulations and the vortices created by the thermal expansion are well captured, which shows that the flame and flow physics of the reference case are correctly reproduced with AMR.
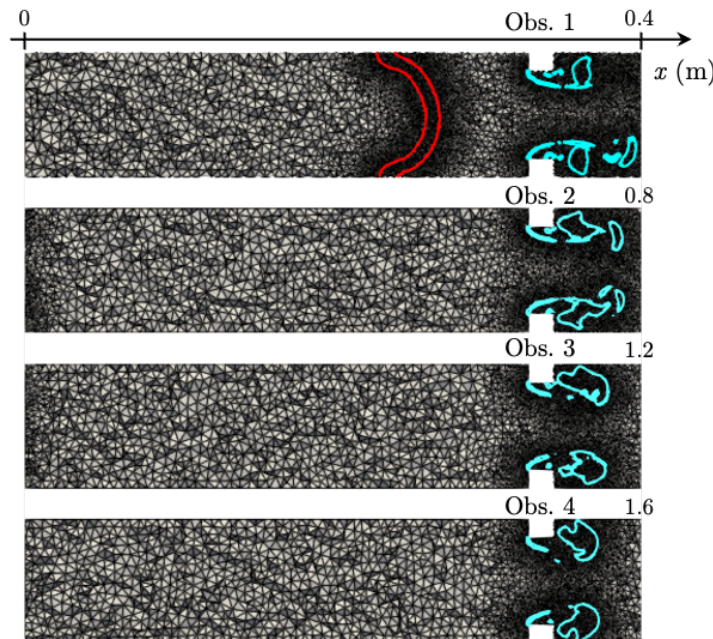

Figure 12: Vertical slice of the mesh at 30 ms. Only the first 1.6 m of the tube are shown here, divided in four parts for a better visualisation. The QoI (flame and vortices) are indicated by contours.
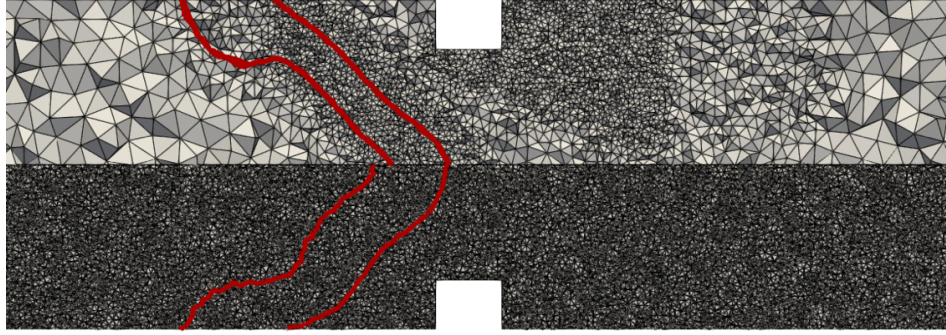
Figure 13: Comparison between the AMR-adapted mesh (top) and the REF static mesh (bottom) at the second obstacle (t = 40 ms). The flame is identified by a flame sensor iso-contour.

The same analysis done for the REF case in Section 4.1 is now performed for the AMR simulation. As shown in Figure 14, the AMR simulation successfully retrieves the correct absolute flame speed evolution. The observed variability remains reasonable considering the highly turbulent nature of the deflagration. The same goes for the overpressure signals, shown in Fig. 15. The evolution is closely retrieved and the maximum overpressure peak, obtained in probe P3, even if lower than the REF case, remains in the experimental range, which is an acceptable result. The difference comes from the higher dissipation of the shock formed by compression waves coalescence when propagating into the coarse regions of the AMR mesh, which have a larger cell size ($\Delta_x = 5$ mm) than the reference mesh in this region. These results could be improved using a shock-based sensor to dynamically refine the shock along its propagation.
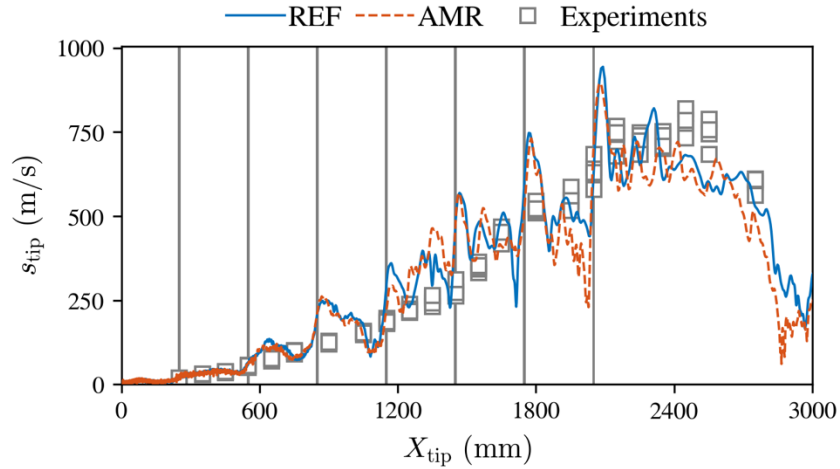

Figure 14: Flame absolute propagation speed s_{tip} with respect to the flame position along the channel X_{tip}. The position of the obstacles is indicated by vertical lines.
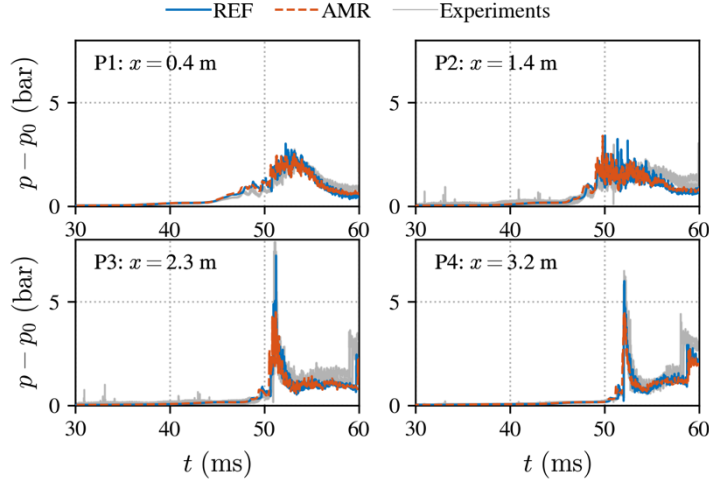
9

Figure 15: Overpressure generated at several probe locations along the channel.

The results in terms of computational cost reduction are also very satisfying. In this case, 88% of the reference case cost is saved by using AMR. This result is mainly due to the significant reduction in the number of cells, whose evolution is shown in Fig. 16. The number of cells in the AMR case is always at least 3.5 times smaller than in the reference case with the static mesh. A total of 1015 mesh adaptations are triggered in the AMR simulation, which correspond only to 25% of the total computational cost.
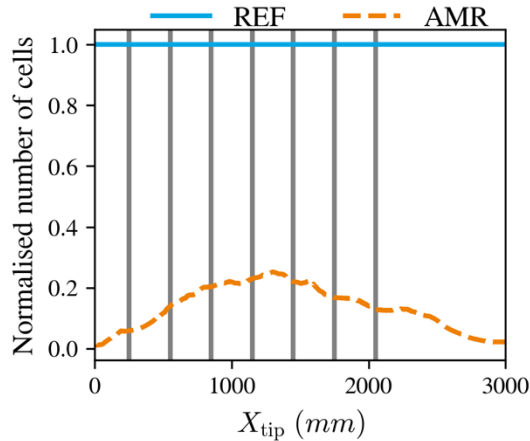

Figure 16: Evolution of the number of cells in the AMR simulation, normalised by the size of the reference static mesh, as a function of the flame tip position. Vertical lines correspond to the obstacles.

5.0 CONCLUSION

LES of deflagrations in the complex GraVent BR30hS300 explosion channel have been performed in order to compare static and AMR strategies. First, an LES on a static mesh showed the capability of the AVBP solver to reproduce the flame and flow physics observed experimentally. Then, the comparison with LES using AMR validates the developed methodology and its ability to reproduce the reference static simulation for a much lower computational cost (88% reduction). This result proves how promising the AMR method presented can be for the LES of propagating turbulent flames, making simulations of large and complex configurations more affordable. This method can be applied as-is in any configuration of explosion in an obstructed environment, where the flame and vortical structures are the key phenomena of interest. In other cases, the AMR methodology can be extended by developing adapted sensors to adequately target the specific QoI of each case.

6.0 ACKNOWLEGEMENTS

7.0 REFERENCES

1. L. Boeck, P. Katzy, J. Hasslberger, A. Kink, and T. Sattelmayer, The gravent ddt database, *Shock Waves* **26** (2016).

2. O. Vermorel, P. Quillatre, and T. Poinsot, Les of explosions in venting chamber: A test case for premixed turbulent combustion models, *Combustion and Flame* **183**, 207 (2017).

3. L. Y. M. Gicquel, N. Gourdain, J. F. Boussuge, H. Deniau, G. Staffelbach, P. Wolf, and T. Poinsot, Calcul parallèle haute performance des écoulements en géométries complexes, *Comptes Rendus - Mecanique* **339**, 104 (2011).

4. P. Lax and B. Wendroff, Systems of conservation laws, *Communications on Pure and Applied Mathematics* **13**, 217 (1960).

5. F. Nicoud and F. Ducros, Subgrid-scale stress modelling based on the square of the velocity gradient tensor, *Flow, Turbulence and Combustion* **62**, 183 (1999).

6. T. Poinsot and S. K. Lele, Boundary conditions for direct simulations of compressible viscous flows, *Journal of Computational Physics* **101**, 104 (1992).

7. O. Colin, F. Ducros, D. Veynante, and T. Poinsot, A thickened flame model for large eddy simulations of turbulent premixed combustion, *Physics of Fluids* **12**, 1843 (2000).

8. P. Haldenwang and D. Pignol, Dynamically adapted mesh refinement for combustion front tracking, *Computers & Fluids* **31**, 589 (2002).

9. S. Sengupta, Ph.D. thesis, INP Toulouse (2023).

10. R. S. Cant, U. Ahmed, J. Fang, N. Chakarborty, G. Nivarti, C. Moulinec, and D. R. Emerson, An unstructured adaptive mesh refinement approach for computational fluid dynamics of reacting flows, *Journal of Computational Physics* **468**, 111480 (2022).

11. C. Lapointe, N. T. Wimer, J. F. Glusman, A. S. Makowiecki, J. W. Daily, G. B. Rieker, and P. E. Hamlington, Efficient simulation of turbulent diffusion flames in openfoam using adaptive mesh refinement, *Fire Safety Journal* **111**, 102934 (2020).

12. J. P. Legier, T. Poinsot, and D. Veynante, Dynamically thickened flame les model for premixed and non-premixed turbulent combustion, *Proceedings of the Summer Program, Centre for Turbulence Research* 157–168 (2000).

13. C. Liu, Y. Wang, Y. Yang, and Z. Duan, New omega vortex identification method, *Science China: Physics, Mechanics and Astronomy* **59** (2016).

14. P. Benard, G. Balarac, V. Moureau, C. Dobrzynski, G. Lartigue, and Y. D'Angelo, Mesh adaptation for large-eddy simulations in complex geometries, *International Journal for Numerical Methods in Fluids* **81**, 719 (2016).

15. C. Dobrzynski and P. Frey, Anisotropic delaunay mesh adaptation for unsteady simulations, *Proceedings of the 17th International Meshing Roundtable* 177–194 (2008).

16. C. Dapogny, C. Dobrzynski, and P. Frey, Three-dimensional adaptive domain remeshing, implicit domain meshing, and applications to free and moving boundary problems, *Journal of Computational Physics* **262**, 358 (2014).

17. F. Alauzet, P. L. George, B. Mohammadi, P. Frey, and H. Borouchaki, Transient fixed point-based unstructured mesh adaptation, *International Journal for Numerical Methods in Fluids* **43**, 729 (2003).

18. O. Dounia, Ph.D. thesis, INP Toulouse (2018).

19. L. Boeck, Ph.D. thesis, Technische Universität München (2015).

20. U. of California at San Diego, Chemical-kinetic mechanisms for combustion applications, (2016), http://combustion.ucsd.edu.

21. D. G. Goodwin, H. K. Moffat, and R. L. Speth, Cantera: An object-oriented software toolkit for chemical kinetics, thermodynamics, and transport processes (2017).